Applied Surface Science 611 (2023) 155622

Contents lists available at ScienceDirect

Applied Surface Science

journal homepage: www.elsevier.com/locate/apsusc

Full Length Article

Functionalizing aerogels with tetraazamacrocyclic copper(II) complexes: Nanoenzymes with superoxide dismutase activity

Norbert Lihi [a,*], Zoltán Balogh [a,b,c], Róbert Diószegi [a,b], Attila Forgács [a], Krisztián Moldován [a,b], Nóra V. May [d], Petra Herman [a], István Fábián [a], József Kalmár [a,*]

[a] ELKH-DE Mechanisms of Complex Homogeneous and Heterogeneous Chemical Reactions Research Group, Department of Inorganic and Analytical Chemistry, University of Debrecen, Egyetem tér 1, Debrecen H-4032, Hungary
[b] Doctoral School of Chemistry, University of Debrecen, Egyetem tér 1, Debrecen H-4032, Hungary
[c] Neutron Spectroscopy Department, Centre for Energy Research, Konkoly-Thege Miklós út 29-33, Budapest H-1121, Hungary
[d] Centre for Structural Science, Research Centre for Natural Sciences, Magyar tudósok körútja 2, Budapest H-1117, Hungary

ARTICLE INFO

Keywords:
Superoxide dismutase
Aerogel
Copper(II)
Cyclen
Cyclam

ABSTRACT

The copper(II) complexes of 1,4,7,10-tetraazacyclododecane (cyclen) and 1,4,8,11- tetraazacyclotetradecane (cyclam) were covalently immobilized in mesoporous silica aerogels by the sol–gel method using functionalized silica precursors. The modified macrocyclic precursors are characterized by mass spectrometry (MS) and solution phase nuclear magnetic resonance (NMR) spectroscopy. The supercritically dried aerogels are characterized using low voltage scanning electron microscopy (LV-SEM), N_2-sorption porosimetry, infrared spectroscopy (FT-IR), electron paramagnetic resonance spectroscopy (EPR) and contrast variation small angle neutron scattering (SANS). The suspended aerogel particles act as nanoenzymes, because they have significant SOD activities, dramatically higher than the corresponding dissolved Cu(II) complexes. The most important factors responsible for the altered reactivities due to the covalent immobilization of the complexes were elucidated based on the compiled results of the characterization methods. These are: *i*) the formation of new chemical environments and Cu(II) coordination modes; *ii*) the effective separation of the active Cu(II) centers in the aerogels; and *iii*) the confinement effect operative in the nanoporous network. As a perspective, the present functionalized aerogel microparticles can be developed into passive targeting antioxidant pharmaceutical agents administered locally or subcutaneously.

1. Introduction

Cellular respiration requires molecular oxygen; however, the incomplete reduction of oxygen leads to the formation of reactive oxygen species (ROS) in biological systems. Antioxidant enzymes such as superoxide dismutases and glutathione peroxidases keep the concentrations of the ROS at controlled low limits. Interestingly, a considerable amount of the oxygen is metabolized through ROS yielding two primary products, superoxide anion radical ($O_2^{\bullet -}$) and hydrogen-peroxide (H_2O_2) [1]. Superoxide dismutase enzymes (SODs) assist the decomposition reaction of superoxide anion radical to molecular oxygen and hydrogen peroxide [2]. SODs are classified on the basis of the transition metal ion found in the active center, such as Cu/Zn-, Mn-, Fe- and Ni-SOD [3]. Indeed, these metal ions facilitate the disproportionation of superoxide anion by cycling between the reduced and oxidized states of the metal ion. The absence of SODs or the high ROS concentration leads to the damage of biomolecules and causes oxidative stress and inflammatory diseases [3–5]. Moreover, elevated ROS concentration can play a significant role in human cancer development due to the inactivation of tumor suppressor genes [6]. Since the direct utilization of native SODs as therapeutic agents is not feasible due to their low solution stability and membrane permeability, significant effort has been made to develop efficient SOD mimicking ROS scavenging systems [7–9]. These mimics usually contain a redox active metal ion in an appropriate coordination environment, or intrinsic radicals that effectively catalyze the decomposition of superoxide anion [10]. Moreover, a promising strategy to improve the recyclability and the stability of the SOD mimics is their immobilization in solid supports [11–13]. As an example, the copper(II) bishistamine complex was immobilized in layered double hydroxide nanoclays containing poly(vinylpyridine-*b*-methacrylic acid). This

* Corresponding authors.
E-mail addresses: lihi.norbert@science.unideb.hu (N. Lihi), kalmar.jozsef@science.unideb.hu (J. Kalmár).

https://doi.org/10.1016/j.apsusc.2022.155622
Received 16 August 2022; Received in revised form 4 November 2022; Accepted 4 November 2022
Available online 9 November 2022
0169-4332/© 2022 The Author(s). Published by Elsevier B.V. This is an open access article under the CC BY-NC-ND license (http://creativecommons.org/licenses/by-nc-nd/4.0/).

nanocomposite exhibited an SOD activity significantly higher than the dissolved complex, because the immobilization altered the coordination geometry of Cu(II) leading to a more active species [14]. Similar findings were reported for the immobilization of bridged Cu(II), Zn(II) diethylenetriamine complexes [15].

Mesoporous silica materials have high apparent surface areas, highly permeable pore networks and good mechanical and chemical stabilities that make them ideal catalyst supports. The catalytic reactions take place in confinement inside the nanosized pores, where the effective frequency of reactive collisions is relatively high. Indeed, phenanthroline based hydroxo-bridged dinuclear Cu(II) complexes, $[(phen)_2Cu(\mu\text{-}OH)Cu(phen)_2]^{3+}$, immobilized in mesoporous silica effectively mimic catechol oxidase activity *via* the oxidation of 3,5-di-*tert*-butylcatechol to the corresponding quinone derivative [16]. An imidazolato-bridged Cu(II)-diethylene-triamino-μ-imidazolato-Zn(II)-tris-(aminoethyl)amine complex was prepared as a functional model of the CuZn-SOD enzyme. The heterodinuclear complex was covalently immobilized in a mesoporous silica support, which is proposed to act as the skeleton of the protein framework, while the Cu(II) center mimics the active site of the enzyme. This composite nanosystem is very stable in aqueous medium and shows persistent SOD activity [17].

In the quest for developing functional antioxidant nanosystems, we have covalently conjugated the copper(II) complexes of 1,4,7,10-tetraazacyclododecane (cyclen) and 1,4,8,11-tetraazacyclotetradecane (cyclam) into mesoporous silica aerogels in this study. These complexes have already been studied as neuroprotective and radiotheranostic agents [18,19]. Specifically, the cyclen and cyclam macrocycles were chosen to ensure the high thermodynamic stability and the kinetic inertness of the coordination of Cu(II), which is essential in biological systems where competitive ligands are abundant in the form amino acids, peptides, proteins and other biomolecules. These are usually present in higher concentrations than the biologically active complexes and can remove the majority of Cu(II) in ligand exchange reactions. Such inactivation of complexes containing open-chain ligands that favor ligand exchange reactions is often observed during *in vitro* cell viability and cell proliferation experiments. The half-lives of the dissociations are 0.87 days for $[Cu(II)\text{-cyclen}]^{2+}$ in 2 M $HClO_4$ at 25 °C and 2.7 days for $[Cu(II)\text{-cyclam}]^{2+}$ in 1 M HCl at 30 °C, respectively [20,21]. Consequently, they are ideal candidates as potential redox active antioxidant systems. The chemical structures of the macrocyclic precursors yielding the active centers in the final aerogels were characterized by several spectroscopic methods. The functionalized aerogels were characterized in their dry states, and after suspending them in aqueous media. The superoxide dismutase activities of these microparticles were studied using the xanthine / xanthine oxidase / nitro blue tetrazolium chloride (NBT) assay. The SOD activities of the functionalized aerogel microparticles were contrasted to those of the corresponding aqueous Cu(II) complexes in order to understand the most important structural features affecting the reactivities of the nanosystems.

Giving the explanation for the effects of the selected covalent immobilization strategies on the reactivities of the two macrocyclic Cu(II) complexes is an additional level of complexity, which is included in the present study.

2. Experimental Section

2.1. Chemicals

Tetramethyl orthosilicate (TMOS), 1,4,7,10-tetraazacyclododecane (cyclen), 1,4,8,11- tetraazacyclotetradecane (cyclam), (3-glycidoxypropyl)-trimethoxysilane (GPTMS), (3-chloropropyl)-trimethoxysilane (CPTMS), *N*,*N*-diisopropyl-ethylamine (DIPEA), and Cu(II) nitrate were purchased from Sigma-Aldrich (Budapest, Hungary). Methanol, acetonitrile and acetone were purchased from Molar Chemicals ltd. (Budapest, Hungary). Ammonium carbonate, ammonium acetate and nitric acid (65 %) were purchased from Merck (Budapest, Hungary). The aqueous solutions were prepared with doubly deionized and ultrafiltered water (ELGA PureLab classic system). Argon gas cylinders (99.996 %) and carbon dioxide cylinders (Biogon-C, 99.5 %) equipped with a dip tube were purchased from Linde Gáz Magyarország Zrt. (Debrecen, Hungary). All liquid chemicals (HNO_3, H_2O_2, HF) that were used for the dissolution of samples preceding ICP-OES measurements, were ACS reagent grade from Sigma-Aldrich. The standard solutions used for the calibration of the ICP-OES were obtained from Scharlau (Barcelona, Spain). Xanthine, xanthine oxidase (0.5 U/mg) and nitro blue tetrazolium chloride (NBT) were purchased from Sigma-Aldrich (Budapest, Hungary).

2.2. Synthesis of functionalized silica aerogels

Copper(II)-cyclen and Cu(II)-cyclam functionalized silica aerogels were prepared using the base catalyzed sol–gel synthesis method adopted from the literature [22,23]. The choice of the ligands limited the synthetic options for immobilization. Unfortunately, the same linkers could not be used for the immobilization of both complexes. In both cases, the synthesis was carried out under inert gas (Ar) atmosphere in order to avoid the reaction of the cyclen and cyclam moieties with CO_2 in air. The complexation of Cu(II) could be achieved in good yields only in the solution phase using the as-prepared macrocyclic precursors.

The synthesis procedures and the chemical structures of the Cu(II)-cyclen and Cu(II)-cyclam functionalized aerogels (CuClen-AG and CuClam-AG, respectively) are discussed in details in Section 3.1. A schematic showing the synthesis steps is also given in that section. The characterization of the synthetic precursors is detailed in the Supporting Information.

2.2.1. Synthesis of Cu(II)-cyclen functionalized aerogel (CuClen-AG)

A mixture of 32 ml (1778 mmol) water and 63.5 ml (1088 mmol) ethanol was added to a two-neck flask, which was flushed with Ar gas before the reaction. 802 mg (4.65 mmol) cyclen was dissolved in the flask, 4.0 ml GPTMS (18.1 mmol) was added to the solution, and the mixture was stirred for 30 min at room temperature. The functionalized silica-precursor formed in the reaction between cyclen and GPTMS. This precursor was characterized by NMR and MS techniques in the solution phase, as detailed in the Supporting Information (Figs. S1–S5). Afterwards, 1.12 g $Cu(NO_3)_2{\cdot}3H_2O$ (4.63 mmol) was dissolved in 20.0 ml (1111 mmol) of water. The $Cu(NO_3)_2$ solution was added to the reaction mixture. Due to complex formation, the color of the solution changed from colorless to dark blue.

The silica gel was prepared by adding 15.2 ml (102.9 mmol) TMOS to the system, followed by the addition of 382 mg (3.97 mmol) of ammonium carbonate as a catalyst dissolved in 4.0 ml (222 mmol) water. The mixture was poured immediately into a plastic mold. Gelation took place within a few minutes. The alcogel was kept in the sealed mold for 5 days. The aged gels were placed into methanol for 24 h. Subsequently, a multistep solvent exchange was performed, as follows. Methanol was replaced to a mixture of methanol-acetone 2:1, methanol-acetone 1:1, and finally to pure acetone. Before the supercritical drying, the gel was soaked in freshly distilled acetone for three days to remove residual water. Drying was performed in a pumpless drying system using supercritical CO_2 according to a previously published protocol [23,24].

2.2.2. Synthesis of Cu(II)-cyclam functionalized aerogel (CuClam-AG)

In a two-necked flask 906 mg (4.43 mmol) cyclam was dissolved in 63 ml (1205 mmol) acetonitrile. Afterward, 5.0 ml (28.0 mmol) DIPEA and 0.83 ml (4.55 mmol) CPTMS was added to the mixture. The solution was refluxed for 24 h under Ar gas atmosphere. After 24 h, the mixture was evaporated to dryness. The as-prepared solid was dissolved in 20.0 ml (492 mmol) methanol. 995 mg (5.30 mmol) of $Cu(NO_3)_2$ was dissolved in the mixture of 12.8 ml (711 mmol) of water and 10.0 ml (246 mmol) of methanol. The precursor was characterized by NMR and MS techniques in the solution phase, as detailed in the Supporting

Information (Figs. S6–S11). When the $Cu(NO_3)_2$ solution was added, a dark purple solution was obtained.

The precursor complex obtained in the previous step was mixed with 15.2 ml (101.6 mmol) of TMOS, 60.0 ml methanol (1476 mmol) and 6.0 ml saturated ammonium acetate solution (0.66 g, 8.56 mmol). The resulting solution was immediately poured into a plastic mold, where gelation took place in a few minutes. The dark purple colored alcogel was aged for 24 h in the mold, then placed into methanol. Subsequently, a multi-step solvent exchange and the supercritical drying was performed using exactly the same protocol as in the case of the Cu(II)-cyclen aerogel.

2.3. Aerogel characterization

2.3.1. Conventional techniques

Scanning electron microscopy (SEM) images were taken in a ThermoFisher Scientific Scios 2 instrument. The electron beam resolution is 1.6 nm at the optimum working distance (<5 mm) at 1 keV accelerating voltage due to the in-lens trinity detection system. Low voltage scanning electron microscopy (LV-SEM) was applied to image the aerogel samples in their pristine states without applying conductive coating to avoid any morphological artefacts. The samples were fixed with a vacuum-resistant carbon tape.

Nitrogen adsorption–desorption porosimetry was performed in a Quantachrome Nova 2200e instrument. Before the measurements, the samples were degassed under vacuum at 80 °C for 24 h. Specific surface area was calculated from the adsorption curve using the BET method. Pore size distribution was calculated from the desorption curve using the BJH method.

The infrared spectra (FT-IR) of the aerogels were measured with a Perkin Elmer Spectrum Two Spectrometer using a universal ATR head (Single Reflection Diamond – L1600607). The IR spectra of the samples were recorded in the range of 450–4000 cm^{-1} at 55–95 % transmittance.

2.3.2. Copper content of aerogels by ICP-OES

In order to solubilize the copper content of the aerogels, different digestion experiments were performed. In the first experiment, 4.00 ml of 65 % HNO_3 and 1.00 ml of 30 % H_2O_2 solutions were added to 10.0 mg powdered aerogel and heated in a high-power microwave system (Milestone EHTOS UP) to 200 °C in 15 min, and kept at high temperature for another 15 min. In the second experiment, an additional 1.00 ml of 40 % HF was added to the above described digesting solution. After microwave heating, 1.00 ml of 45 g/L boric acid solution was added to this sample and heated again. The digested samples were brought to 25.0 ml final volume by ultrapure water. In the first experiment, the silica residues were removed by centrifugation. In the second experiment, the aerogels were completely solubilized.

The copper concentrations of the solutions were measured by ICP-OES using an Agilent 5100 SVDV spectrometer. Five-point matrix fitted calibration was applied, diluted from 1000 mg/L certified copper standard solution. Emission intensity was measured at 327.395 nm. Measuring parameters were as follows: read time: 5 s; uptake delay: 15 s; rinse time: 30 s; stabilization time: 10 s, viewing height: 8 mm, the nebulizer gas flow rate: 0.70 L/min, plasma gas flow rate: 12.0 L/min. SVDV viewing mode was applied. The concentrations of at least 3 parallel samples were averaged.

2.3.3. Hydrolytic stability of the functionalized aerogels

The possibility of the liberation of Cu(II)-species from the functionalized aerogels was tested by mixing the aerogels with appropriate buffers in the pH range between 4.05 and 9.85. The aerogel concentration of the suspensions was 1 mg/mL. The experiments were carried out at 25 °C and 37 °C, and the samples were agitated with a magnetic stirrer for a maximum of 8 h. The samples were centrifuged for 20 min at 4700 rpm (VWR MEGASTAR 1.6 R), the supernatant was separated from the pellet, and the copper contents were analyzed using ICP-OES. In those cases where the copper content of the supernatant was not zero, UV–vis spectra were recorded in a Cary-60 (Agilent Technologies) instrument. These UV–vis spectra were contrasted to those of aqueous Cu (II), $[Cu(II)\text{-cyclen}]^{2+}$ and $[Cu(II)\text{-cyclam}]^{2+}$.

2.3.4. Small angle neutron scattering (SANS)

The experiments were performed on the Yellow Submarine SANS instrument at the Budapest Neutron Center (BNC), as described in previous publications [25,26]. The aerogels were measured in their pristine states, and subsequently, filled with a 66 (V/V)% H_2O – 34 (V/V)% D_2O mixture for varying the contrast, as discussed later.

The momentum transfer (Q) is defined by the following equation:

$$Q = \frac{4\pi}{\lambda}\sin\frac{\theta}{2} \tag{1}$$

λ is the wavelength of the monochromatic neutron beam and Θ is the scattering angle. The Q range of 0.0055–0.4000 $Å^{-1}$ was covered. The recorded scattering intensity was corrected for sample transmission, empty cell scattering, detector sensitivity and background scattering. The Beaucage model was used for fitting the corrected intensity versus scattering vector ($I(Q)$) curves. The 2-level Beaucage model covers the whole experimental Q range [27,28]

$$\mathrm{I(Q)} \cong G_1\exp\left(-\frac{Q^2R_{g1}^2}{3}\right) + B_1 exp\left(-\frac{Q^2R_{g2}^2}{3}\right)\left(\frac{\left[erf\left(\frac{QR_{g1}}{\sqrt{6}}\right)\right]^3}{Q}\right)^{p_1} + G_2\exp\left(-\frac{Q^2R_{g2}^2}{3}\right) + B_2 exp\left(\frac{\left[erf\left(\frac{QR_{g2}}{\sqrt{6}}\right)\right]^3}{Q}\right)^{p_2} + C \tag{2}$$

Here, R_{g1} and R_{g2} are mean gyration radii, p_1 and p_2 are the power exponents at the different structural levels, while G_1, G_2 and B_1, B_2 are treated as adjustable scaling parameters, and C is the incoherent scattering treated as the background. The R_g parameter is representative for the mean pore size in the case of mesoporous and macroporous silica aerogels. When the general pore geometry is approximately cylindrical, the mean pore size (d_{pore}) can be calculated from R_g as follows [27,28]

$$d_{pore} = 2r_{pore} \cong 2\sqrt{\frac{12}{7}}R_g \tag{3}$$

Data fitting was performed using the non-linear Levenberg-Marquardt least-squares algorithm in the SasView 5.0.3 open source, collaboratively developed software.

2.3.5. Size distribution and Zeta potential of aerogel particles

The dry aerogel samples were wet ground in the appropriate aqueous media using a Potter-Elvehjem tissue grinder for 5 min. The resulting suspension was sonicated (ARGO LAB DU-32) for 15 min and then stirred for 20 min at 300 rpm using a magnetic stirrer and a 1.0 cm Teflon-coated rod. This ensures the highly reproducible production of aerogel suspensions that do not settle or aggregate in the time scale of the experiments.

The size distribution of the hydrated aerogel microparticles was measured using a microscope hemocytometer. Images were taken from $c_{Agel} = 0.5$ mg/ mL suspensions with a 1.3 MP microscope camera, and the size distribution of the aerogel particles was determined using the ImageJ software for analysis.

The Zeta potential values of the particles were measured between pH = 3.0 and 9.0 ($c_{Agel} = 1.0$ mg/ mL). The pH of the suspensions was adjusted by adding diluted HCl or NaOH solutions. No background electrolyte was used. The measurements were performed in a MALVERN Zetasizer Nano ZS instrument using the automatic instrument setup and alignment option. All calculations were performed by the instrument

controlling software.

2.3.6. Electron paramagnetic resonance (EPR) spectroscopy

The EPR spectra of the functionalized aerogels and the corresponding hydrated complexes were recorded as described in a previous publication [25]. The aerogels were investigated in their dry states and in aqueous suspensions. For the frozen solution measurements, 0.2 ml sample was mixed with 0.05 ml MeOH in a quartz EPR tube and cooled to 77 K. The dry samples were investigated at room temperature.

X-band CW-EPR spectra were recorded with a BRUKER EleXsys E500 spectrometer. The acquisition parameters were as follows: microwave frequency 9.4 GHz, microwave power 13 mW, modulation amplitude 5 G, modulation frequency 100 kHz. The recorded spectra were corrected by the baseline measured in an identical way and simulated using a

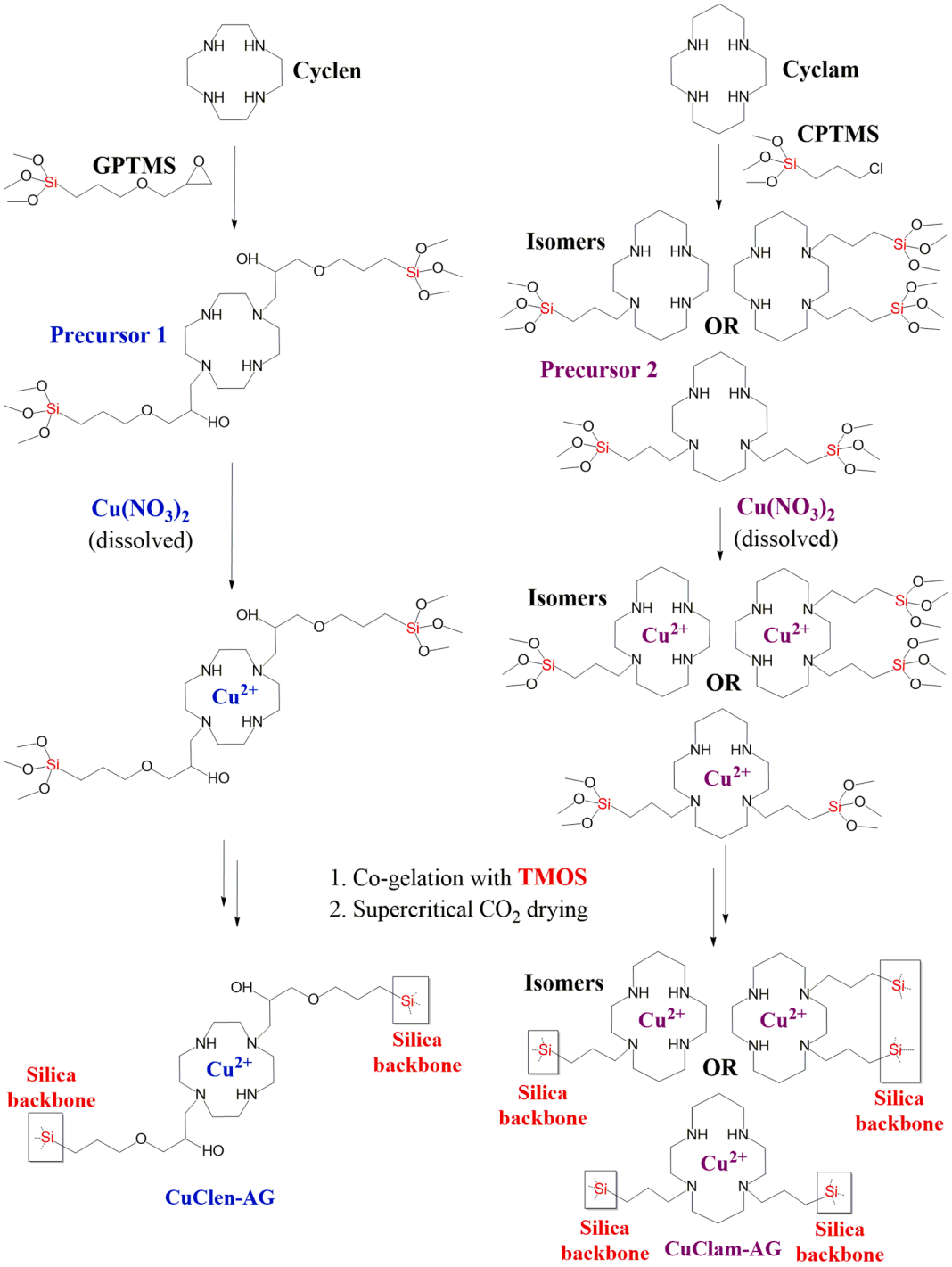

Scheme 1. The preparation steps and the chemical structures of the synthetic precursors, and the Cu(II)-cyclen and Cu(II)-cyclam functionalized aerogels (CuClen-AG and CuClam-AG, respectively). The combined MS and NMR [^{1}H NMR, ^{1}H–^{1}H COSY, ^{1}H–^{1}H TOCSY and (^{1}H,^{13}C)-HSQC] characterization of the synthetic precursors is detailed in the Supporting Information. The coordination modes of Cu(II) in the functionalized aerogels were studied by EPR as detailed in Section 3.8. In the case of CuClen-AG, the macrocycle is attached to the silica backbone via two linkers in *trans* position. In the case of the CuClam-AG, the majority of the macrocycle is attached via two linkers in the form of the two *cis* position isomers. A minor portion of the cyclam macrocycle can be present in attachment via one linker.

dedicated EPR program [29]. The axial ***g***-tensor ($g_{\|}$ and $g_{\perp}$) and the copper hyperfine ***A***-tensor ($A_{\|}$ and $A_{\perp}$) were used for simulating the components. The super-hyperfine coupling of the coordinated nitrogen atoms is not resolved in the spectra, but they have a significant line broadening effect. Therefore, the couplings of 4 equivalent isotropic nitrogen atoms were taken into account for simulating the spectra. The linewidths were fitted using axial linewidth parameters ($\omega_{||}$, $\omega_{\perp}$). The spectra were calculated as the sum of the spectra of the ^{63}Cu and ^{65}Cu weighted by their natural abundances.

2.4. SOD activity measurements

The dismutation reaction of the superoxide anion catalyzed by the functionalized aerogel microparticles or the corresponding dissolved Cu(II) complexes was quantitatively studied using the xanthine / xanthine oxidase / NBT assay. In this reaction system, the oxidation of xanthine to uric acid by xanthine oxidase produces the superoxide anion radical ($O_2^{\bullet-}$). The radical *in situ* reduces the nitro blue tetrazolium chloride (NBT) detector molecule into diformazan. The formation of diformazan is followed by UV–vis spectrophotometry at 560 nm with high sensitivity. The addition of an SOD mimic to this reaction system lowers the steady-state concentration of superoxide decreasing the rate of the formation of diformazan.

The assay was carried out in phosphate buffer (pH = 6.45 and 7.60; c = 0.05 M) containing 45 μM NBT and 200 μM xanthine at 25 and 37 °C. At pH 6.45, the SOD activity measurements were carried out only at 37 °C, since the rate of the superoxide production i.e., the formation of diformazan is relatively slow at 25 °C. The reaction was initiated by adding an appropriate amount of xanthine oxidase to set a ca. 0.020 min^{-1} rate of absorbance increases at 560 nm. First, the reaction was monitored in a control sample without the addition of any SOD mimic. In the test samples, the reaction was started, let to run for 4.0 min, then the SOD mimic was added, and the system was monitored further for 4.0 min. The original and the altered rates of the absorbance increase were estimated by fitting the appropriate parts of the kinetic curves with linear (zeroth order rate) functions. The calculations for estimating the inhibition parameters were performed using the conventional method reported in the literature [30,31]. The SOD activities of the aerogels and the complexes are expressed in molar copper-concentration equivalent IC_{50} values [32].

3. Results and discussion

3.1. Chemical structures of aerogels

The synthetic steps yielding the macrocyclic precursors and the final functionalized aerogels are shown in Scheme 1. The chemical structures of the synthetic precursors were determined experimentally. Following the attachment of the GPTMS based arms to cyclen and the CPTMS based arms to cyclam, the synthetic precursors were isolated, re-dissolved in the appropriate solvents and characterized by NMR [^{1}H NMR, ^{1}H–^{1}H COSY, ^{1}H–^{1}H TOCSY and (^{1}H,^{13}C)-HSQC] and MS techniques in the solution phase. The detailed results are given in the Supporting Information. As a summary, the reaction of cyclen with excess GPTMS results in the formation of a single product, where two GPTMS based arms are attached to the *N*-atoms of the cycle in *trans* position. Neither the formation of the *cis* product, nor the variation of the number of the side arms was detected in any of the MS and the NMR spectra. The reaction of cyclam with a quasi-stoichiometric amount of CPTMS yields multiple products. According to the compiled results of the MS and the 2D NMR experiments, the majority of the products contain two CPTMS based arms attached to cyclam. Interestingly, the two arms are not attached to the *N*-atoms in *trans* position. Only the *cis* isomers were detected, however, their proportions could not be quantified. Additionally, the formation of minor isomeric products with a single CPTMS based arm cannot be ruled out.

The incorporation of Cu(II) could be realized with high yield only in this stage of the synthesis procedures using the dissolved macrocyclic precursors. Therefore, the as-prepared solid aerogels already contained Cu(II), which prevented their structural analysis by solid-state NMR spectroscopy. However, the coordination modes of Cu(II) in the functionalized aerogels were elucidated using EPR spectroscopy, and the extracted spin-Hamiltonian parameters unambiguously confirm that the Cu(II) ions are accommodated by the macrocyclic cavities in both aerogels. The complete EPR study is detailed later in Section 3.8.

Based on the compiled results of the characterization of the synthetic precursors and the pristine aerogels, the chemical structures of the functionalized aerogels are as follows. In the case of CuClen-AG, the macrocycle is attached to the silica aerogel backbone via two linkers bound to the *N*-atoms in *trans* position. In the case of the CuClam-AG, the majority of the macrocycle is also attached via two linkers, but in the form of the two *cis* position isomers. A minor portion of the cyclam macrocycle can be present in attachment via one linker, again in the form of isomers. These considerations are reflected in the depicted structures in Scheme 1. The presence of the linkers can alter the reactivities of the immobilized Cu(II)-complexes compared to the dissolved ones, which is discussed in details in Section 3.10.

3.2. Morphology of aerogels

Representative SEM images of CuClen-AG and CuClam-AG are shown in Fig. 1. The studied aerogels are built from primary nanoparticles of spherical shape. These nanoparticles interconnect and form a solid backbone, which defines an open porous network. This architecture is characteristic for silica aerogels [26,33]. The pore sizes are mainly in the mesopore range, but visible macropores are present in both aerogel structures. In the case of the CuClen-AG, the primary nanoparticles are larger and the number of macropores is higher, while the surface of CuClam-AG is coarser. The morphological differences are due to the application of different base catalysts in the sol–gel synthesis of the aerogels (i.e. CuClen-AG: ammonium carbonate; CuClam-AG: ammonium acetate). Basicity determines the rates of the hydrolysis and polycondensation reactions that in turn determine the final size distribution of the primary nanoparticles and the fractal structures of the silica backbones [34].

Representative N_2 adsorption–desorption isotherms are shown in Fig. 2A. For both aerogels, the isotherms are classified as IUPAC type IV with H3 hysteresis loops. This is characteristic for such mesoporous materials that also display a low fraction of macropores [35]. The difference between adsorption and desorption isotherms around $p/p_0 = 0.3$ indicates minor microporosity, and the sharp elevation of the adsorption isotherm at $p/p_0 > 0.9$ is characteristic for the presence of macropores in both aerogels [35].

The estimated structural parameters are listed in Table 1, and the pore size distribution curves are shown in Fig. 2B. Based on the SEM images and the N_2-sorption data, CuClam-AG is a typical mesoporous silica aerogel with a high specific surface area and an open pore network. The porosity, the apparent surface area and the cumulative pore volume of CuClen-AG are significantly lower than those of CuClam-AG. The wide pore size distribution is indicative for the presence of macropores in CuClen-AG. The morphological differences revealed by the N_2-sorption data are well-related to the application of the different base catalysts in the sol–gel procedures, as discussed above [34].

3.3. Small angle neutron scattering (SANS)

The experimental scattering curves together with the results of the non-linear fitting are shown in Fig. 3. The Beaucage model (eq. (2)) was adequate for fitting the data in the whole Q range for the pristine aerogels. The neutron scattering length density (SLD) of amorphous silica (1.96×10^{-6} Å^{-2}) is matched by a 66 (V/V)% H_2O – 34 (V/V)% D_2O (64 wt% H_2O – 36 wt% D_2O) mixture. The pores of the aerogels were

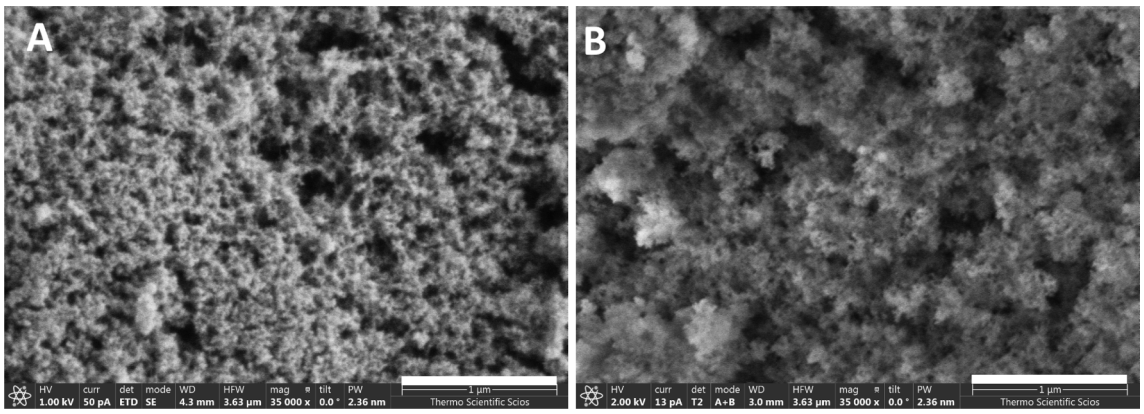

Fig. 1. Low voltage scanning electron microscopy (LV-SEM) images of pristine CuClen-AG (A) and CuClam-AG (B) in 35 k × magnification (scale bar: 1 µm).

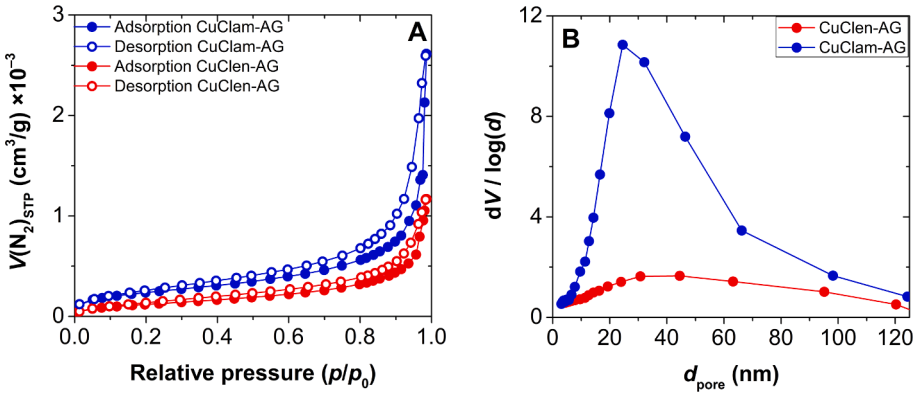

Fig. 2. Panel A: Nitrogen adsorption–desorption isotherms of CuClen-AG (red) and CuClam-AG (blue) aerogels. Panel B: Pore size distributions calculated using the BJH method. The estimated structural parameters are listed in Table 1. (For interpretation of the references to color in this figure legend, the reader is referred to the web version of this article.)

Table 1
Structural parameters of CuClen-AG and CuClam-AG estimated by the BET and the BJH methods from the N_2 adsorption–desorption porosimetry data in Fig. 2.

	CuClen-AG	CuClam-AG
Specific surface area (m^2/g)	464 ± 33	874 ± 69
C-constant	35 ± 2	67 ± 5
Pore volume ($cm^3\ g^{-1}$)	1.7 ± 0.1	3.9 ± 0.4
Mean pore size (nm)	45 ± 2	43 ± 3

completely filled with this fluid in order to shift the contrast, as detailed previously [26,36]. The corresponding SANS curves show practically no specific scattering, which is due to the matching of the backbone. These curves were fitted with an empirical single power-law function that yields a single *p* value [37]. The estimated structural parameters for the pristine and filled aerogels are listed in Table 2.

For hierarchical systems, the scattering of multiple structural levels can appear in the different regions of the experimental *Q* range. In the case of the pristine aerogels, two structural levels are reflected in the SANS curves. The first level in the low *Q* range corresponds to the larger

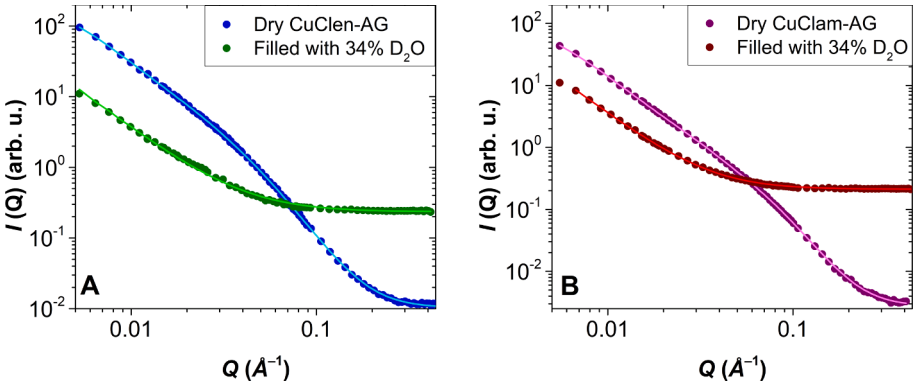

Fig. 3. Small angle neutron scattering (SANS) curves of CuClen-AG (A) and CuClam-AG (B) samples; first measured in their pristine sates (Dry) and later filled with 66(V/V)% H_2O – 34(V/V)% D_2O mixture (Filled). Markers: experimental data; continuous lines: non-linear fitting, as detailed in the text. The calculated parameters are listed in Table 2.

Table 2
Structural parameters estimated by fitting the SANS curves of the different CuClen-AG and CuClam-AG samples in Fig. 3 with the Beaucage or the power-law models.

	Beaucage model						Power-law model
	R_{g1} (Å)	$d_{1\ pore}$ (nm)[a]	p_1	R_{g2} (Å)	$d_{2\ pore}$ (nm)[a]	p_2	p
Pristine CuClen-AG	368 ± 96	96	3.7 ± 0.3	85 ± 4	22	3.48 ± 0.02	
Filled CuClen-AG							1.94 ± 0.01
Pristine CuClam-AG	344 ± 15	90	2.79 ± 0.04	55 ± 5	15	3.77 ± 0.08	
Filled CuClam-AG							2.19 ± 0.01

[a] Calculated from the R_g values using eq. (3).

elements in the micrometre scale. The second level in the middle and low Q ranges corresponds to the nanostructures of the aerogels [27]. The applied Beaucage model is able to describe such structures consisting of multiple hierarchical elements. In eq. (2), R_{g1} and R_{g2} are related to the mean macropore and mesopore sizes, respectively. The mean mesopore size of CuClen-AG is 22 nm and that of CuClam-AG is 15 nm. These values are in reasonable agreement with the pore sizes calculated from the N_2-desorption isotherms. The average macropore size is 96 nm for CuClen-AG and 90 nm for CuClam-AG. Parameter p_1 is characteristic for the microstructure of the aerogel, while p_2 reflects the fractal structure of the network of the primary nanoparticles forming the aerogel backbone [38]. The p_2 values of 3.5 (CuClen-AG) and 3.8 (CuClam-AG) are characteristic for surface fractals. This is in agreement with the main structural feature of the aerogels, i.e., spherical nanoparticles forming a mixed mesoporous and macroporous nanoscale network. The p_1 value is 3.7 for CuClen-AG, which is characteristic for surface fractals and reflects the presence of a number of large macropores with rough surfaces. The p_1 value for CuClam-AG is 2.8, which is characteristic for mass fractals indicating a coarse but homogeneously porous microstructure. These results are in good agreement with the SEM and the N_2-sorption data.

Considering that the contrast of the silica backbones of both of the functionalized aerogels can be matched by the appropriate H_2O – D_2O mixture points out that the immobilized Cu(II)-complexes do not form nanosized clusters in the aerogel backbones. If there were nanosized structural elements enriched in Cu(II), a marked specific scattering were expected from the Cu(II)-clusters even in the case of an appropriate contrast match for silica. Due to the absence of specific scattering, the contrast variation SANS suggests that both the immobilized Cu(II)-cyclen and Cu(II)-cyclam complexes are dispersed homogeneously in the backbones of the aerogels. This is further verified by the EPR results, as discussed later.

3.4. Infrared spectroscopy (IR)

The FT-IR spectra of the aerogels confirm their successful functionalization (Fig. 4). The IR spectrum of a pristine silica aerogel is also shown as reference. The intensive broad band visible in all spectra at around 1050 cm^{-1} is of the Si–O–Si antisymmetric stretching vibration, which is typical for silica aerogels [23]. Two weak bands are present between 2870 and 2950 cm^{-1} in the spectra of the functionalized aerogels that are absent in the case of the pristine silica aerogel. These peaks are characteristic for aliphatic C—H stretching vibrations and originate from the macrocyclic moieties, which proves the successful functionalization of the aerogels with the Cu(II) complexes.

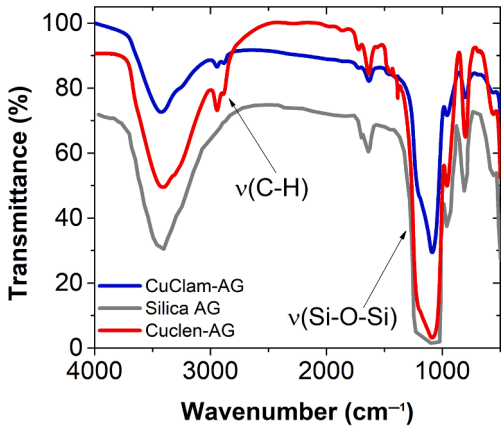

Fig. 4. Infrared spectra (FT-IR) of the pristine CuClen-AG (red), CuClam-AG (blue) and silica (grey) aerogels. (For interpretation of the references to color in this figure legend, the reader is referred to the web version of this article.)

3.5. Copper content of aerogels

The results of the ICP-OES analysis of the functionalized aerogels using different digestions are detailed in Table 3. The two aggressive chemical digestions provided similar results. All immobilized copper was liberated from the functionalized aerogels, even when the silica was not completely solubilized. The copper content of CuClen-AG is around 1.56(m/m)% and that of CuClam-AG is around 1.10 %. These copper contents were used in the calculations in the SOD activity measurements (*vide infra*).

3.6. Hydrolytic stability of the complexes

No leaching of copper was detected from the functionalized aerogels at basic and neutral pH in 8 h at 37 °C. In slightly acidic buffers, copper was detected in the supernatants by ICP-OES. A maximum of 11 % of the copper content of CuClen-AG and a maximum of 26 % of that of CuClam-AG was released at pH = 4.0 in 8 h at 37 °C, as shown in Fig. S12 in the Supporting Information. No further leaching was detected in longer time. The corresponding UV–vis spectra of the supernatants (Fig. S13 in the Supporting Information) clearly show that the liberated Cu(II) species are the respective macrocyclic complexes in both cases, and not free (aqueous) Cu(II). Thus, the hydrolytic stability of the complexes are sufficiently high, but the amorphous silica backbone can hydrolyze to a small extent in acidic solutions that can result in the detachment of the side arms of the macrocyclic complexes leading to their dissolution.

3.7. Zeta potential and particle size distribution

The Zeta potentials of the functionalized aerogels are shown in Fig. 5A as a function of pH. The Zeta potential of the aerogel particles is positive in acidic media, it is close to zero at around neutral pH and negative under alkaline conditions. The Zeta potential of CuClen-AG is slightly higher than that of CuClam-AG in the whole pH range, which is

Table 3
The copper contents of the functionalized aerogels determined using different digestion reactions and subsequent ICP-OES analysis.

	CuClen-AG	CuClam-AG	CuClen-AG	CuClam-AG
Digestion conditions	$HNO_3 + H_2O_2$		$HNO_3 + H_2O_2$ + HF	
copper content (m/m %)	1.53 ± 0.01	1.07 ± 0.03	1.59 ± 0.03	1.13 ± 0.05

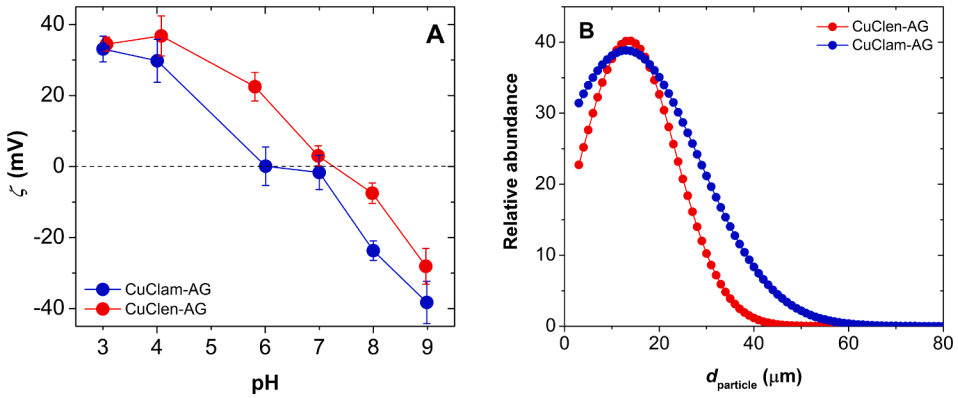

Fig. 5. Panel A: The Zeta potentials of the hydrated CuClen-AG (red) and CuClam-AG (blue) microparticles as a function of pH. Panel B: Size distribution of the hydrated aerogel microparticles. (For interpretation of the references to color in this figure legend, the reader is referred to the web version of this article.)

due to the higher concentration of the immobilized positively charged Cu(II) complexes in CuClen-AG as seen in Table 3. Both aerogels lack functional groups that can lose hydrogen ions at higher pH. Therefore, the negative Zeta potential under alkaline conditions is attributed to the specific sorption of anions on the surface of the particles. Naturally, the specific sorption of anions is facilitated by the large number of positively charged functional groups in the aerogels.

Amorphous silica aerogels tend to spontaneously erode in aqueous media and form stable suspensions of microparticles, as discussed in details in previous publications [33,39]. The present functionalized aerogels erode in a manner that is very similar to the properties of the previously investigated silica aerogels. The size distributions of the stable CuClen-AG and CuClam-AG microparticles are shown in Fig. 5B. The distribution curves are wide with mean sizes of ca. 16 μm for both aerogels, which is typical for non-heat-treated silicas.

3.8. EPR spectroscopy

The EPR spectra of the dry and the hydrated aerogels together with the results of the simulations are shown in Fig. 6. During synthesis, the addition of aqueous Cu(II) yields drastic changes in the UV–vis spectra of the precursor ligand solutions. In line with this, the EPR results clearly show the presence of the expected Cu(II) species in both systems in the resulting dry aerogels. The obtained spin-Hamiltonian parameters confirm that the Cu(II) ions are bound to the respective macrocyclic cavities, and the EPR parameters correspond well to those obtained for the original $[Cu(II)\text{-cyclam}]^{2+}$ and $[Cu(II)\text{-cyclen}]^{2+}$ complexes. The detailed evaluation of the EPR measurements is as follows.

The EPR spectrum of the powdered pristine CuClam-AG recorded at room temperature supports that the Cu(II) complex is immobilized and randomly oriented on the silica surface. The spectrum exhibits one exclusive species characterized by an axial ***g***-tensor considering the usual elongated octahedral geometry of Cu(II). The coupling of 4 equivalent nitrogen atoms in the equatorial sphere of the Cu(II) was taken into account to describe the linewidth. The EPR parameters are in good agreement with those reported previously for Cu(II)-cyclam complexes in frozen solution (Table 4) [40]. The lines of this component are somewhat broad, because the Cu(II) centers are physically close to each other in the aerogels and the interactions between them result in line broadening. However, these centers are not close enough to cause an antiferromagnetic coupling. Similar effects were observed for Cu(II)-cyclen functionalized aerogels, as discussed in the literature [25].

The EPR spectrum of the frozen suspension of the hydrated CuClam-AG cannot be assigned to a single axial ***g***-tensor. The parameters can

Table 4
Anisotropic EPR parameters obtained in the simulation of the EPR spectra in Fig. 6. The SD is ± 0.001 for $g_\perp$ and $g_\parallel$ and ± 1 × 10^{-4} cm^{-1} for $A_\perp$ and $A_\parallel$.

	$g_\perp$	$g_\parallel$	$A_\perp$ [10^{-4} cm^{-1}]	$A_\parallel$ [10^{-4} cm^{-1}]
CuClam-AG	2.040	2.175	25	197
CuClen-AG Component 1[a]	2.049	2.194	17	190
CuClen-AG Component 2[a]	2.056	2.211	10	171
$[Cu(cyclam)]^{2+}$ [b]	2.049	2.186		205
$[Cu(cyclen)]^{2+}$ [b]	2.057	2.198		184

[a] Data are taken from Ref. [25] [b] Data are taken from Ref.[40].

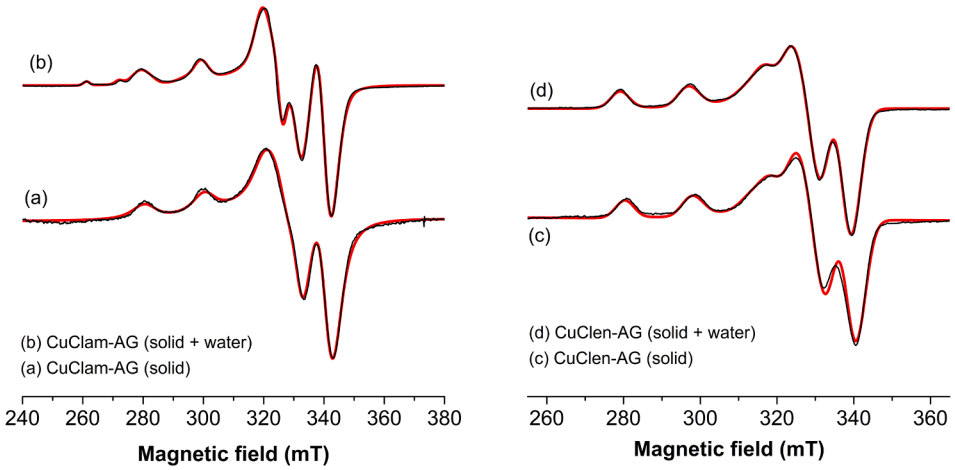

Fig. 6. Experimental (black) and simulated (red) EPR spectra. The spectrum of CuClam-AG at room temperature (a); and the frozen suspension of the hydrated aerogel (b). Spectrum (a) was fitted with the axial EPR parameters reported in Table 4 (CuClam-AG) in 100 %; and spectrum (b) with 90 % CuClam-AG + 10 % Cu^{2+}. The spectrum of CuClen-AG at room temperature (c); and the frozen suspension of the hydrated aerogel (d). Spectrum (c) was fitted with 54 % Component 1 + 46 % Component 2 and (d) with 62 % Component 1 + 38 % Component 2 in Table 4. (For interpretation of the references to color in this figure legend, the reader is referred to the web version of this article.)

adequately be fitted only by considering 2 components. The EPR parameters of the first component is the same as the one found in the powder spectrum, and this species is the major one with 90 % contribution. Beside this complex, the EPR spectrum shows the signal of liberated, aqueous Cu(II), however, this free Cu(II) can exclusively be observed in the frozen samples. Most likely, the freezing shifts the equilibrium between the free and the bound Cu(II), and damages the aerogel structure, as well.

Both the dry powder and the frozen suspension spectra of CuClen-AG suggest that the immobilization of Cu(II)-cyclen in the aerogel leads to the formation of a new Cu(II) complex species (Component 2) next to the complex that is well related to the free Cu(II)-cyclen (Component 1). The corresponding EPR parameters are listed in Table 4. The large $g_{\|}$ and small $A_{\|}$ parameters of Component 2 suggest a weaker equatorial ligand field. In this new complex, most probably, one of the nitrogen atoms is not involved in the binding of Cu(II), and it is possibly replaced by the hydroxyl group of the linker side chain, which was observed in previous cases, as well [25]. The same scenario is not operational for the CuClam-AG, thus, it is reasonable to assume that the coordination sphere of Cu(II)-cyclam is not altered upon immobilization.

3.9. Superoxide dismutase (SOD) activity

Several control experiments were performed to ensure the reliability of the indirect xanthine / xanthine oxidase / NBT assay for the quantification of the SOD activity of the functionalized aerogel microparticles. First, pristine silica aerogel microparticles were tested, and it was confirmed that the silica aerogel does not exhibit any SOD activity. Then, the possibility of side reactions between the reactants and the functionalized aerogels were tested. It was confirmed that the functionalized aerogels do not inhibit the production of the superoxide anion by xanthine oxidase, i.e., the rate of the conversion of xanthine to uric acid is the same in the presence and in the absence of the complexes. It was also confirmed that the NBT detector molecule is not reduced by the functionalized aerogels.

The Cu(II)-complexes of the synthetic precursors containing the silane side arms (cf. Scheme 1) were isolated before adding TMOS, but dissolving these complexes in water and adding them to the aqueous reaction system of the xanthine / xanthine oxidase / NBT assay caused turbidity. This could be due to the hydrolysis and condensation of the silane groups in the side arms. Therefore, these systems cannot serve as solution phase controls for SOD activity.

The inhibition values of the functionalized aerogels and the dissolved $[Cu(II)\text{-cyclam}]^{2+}$ measured at 25 °C and pH = 7.60 are given as a function of the Cu(II) concentrations in the complexes in Fig. 7. Additional inhibition curves obtained at 37 °C, and at pH = 6.45 are reported in Figs. S14–S16 in the Supporting Information. The measured inhibition values are summarized in Table 5. The inhibition values of similar systems reported in the literature are collected in Table 6 for reference.

Table 5
The IC_{50} (μM) values of aqueous and immobilized SOD mimetic systems studied in this work.

pH	pH 7.60		pH 6.45
T	37 °C	25 °C	37 °C
$[Cu(II)\text{-cyclam}]^{2+}$	0.8 ± 0.1	26.1 ± 0.8	0.42 ± 0.08
$[Cu(II)\text{-cyclen}]^{2+}$	N.A.	N.A.	N.A.
CuClam-AG (immobilized Cu(II)-cyclam)	0.20 ± 0.07	1.7 ± 0.1	0.09 ± 0.01
CuClen-AG (immobilized Cu(II)-cyclen)	4 ± 1	2.1 ± 0.2	0.61 ± 0.01

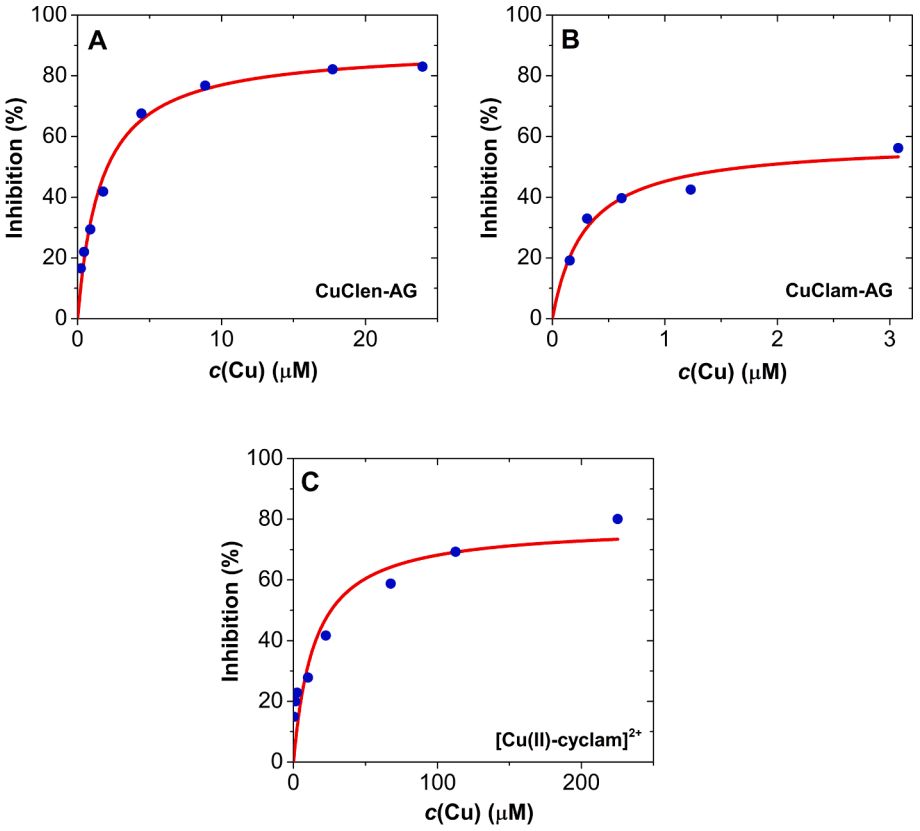

Fig. 7. Inhibition percentage in the xanthine / xanthine oxidase / NBT assay as a function of the copper concentration using CuClen-AG (A), CuClam-AG (B) and aqueous $[Cu(II)\text{-cyclam}]^{2+}$ (C) at 25 °C and pH 7.60. The relative standard deviation (RSD) of the inhibition percent values arising from the uncertainty of the kinetic data is ca. 10 %.

The first important observation is that the aqueous [Cu(II)-cyclen]$^{2+}$ complex does not exhibit any SOD activity. Consequently, the SOD activity of the CuClen-AG microparticles certainly arises due to the immobilization of the Cu(II)-cyclen complex.

The results clearly demonstrate that the functionalized aerogel microparticles show excellent performance in the degradation of superoxide anion. This effect is more pronounced at pH 6.45, however, it is important to note that the rate of the non-catalyzed disproportionation of superoxide also increases by decreasing the pH. When benchmarked against several previously reported aqueous Cu(II) complexes and nanoparticle immobilized Cu(II) species, the present aerogels display higher, or at least comparable performance [9,13,17,41]. Furthermore, the present aerogel microparticles are biocompatible and do not pose the risk of nanotoxicity, as discussed later.

3.10. Reactivity of covalently immobilized Cu(II) complexes

The IC_{50} of the CuClam-AG is one order of magnitude smaller than that of the dissolved [Cu(II)-cyclam]$^{2+}$, demonstrating a significant increase in the SOD activity due to the covalent immobilization. However, it is important to note that complete inhibition was not reached by the CuClam-AG in the concentration range used in this study. In order to account for the increased SOD activity of CuClam-AG compared to aqueous [Cu(II)-cyclam]$^{2+}$, several factors have to be considered. First, the chemical structure of the complex, and thus, the molecular environment of Cu(II) is different in the aerogel due to the covalent linkers, which is further complicated by the existence of isomers, as detailed in Section 3.1. However, new coordination modes were not detected in the as-prepared aerogel by EPR, as detailed in Section 3.8. Second, the Cu(II)-cyclam moieties are molecularly dispersed in the highly permeable aerogel network, as shown by SANS and EPR. This ensures the accessibility of the catalytically active sites, while exerts a confinement effect on the nanoscale curved pore walls [22,25]. Third, on the basis of coordination chemical considerations, immobilization stabilizes the activated form of the complex that forms in the reaction with superoxide radical and inhibits any intermolecular side reactions between these reactive intermediates. An additional factor is the Zeta potential of the CuClam-AG particles. This is only slightly negative at the experimental conditions used for the SOD activity studies, which does not hinder the transport of superoxide, and it is a further advantage under biological conditions.

The increase of the SOD activity as a result of the covalent immobilization is even more profound in the case of CuClen-AG compared to aqueous [Cu(II)-cyclen]$^{2+}$. In this aerogel, the two linkers again alter chemical structure of the complex, and thus, the molecular environment of Cu(II). Here, the EPR data unambiguously show the formation of a new Cu(II) complex species in the case of the immobilized Cu(II)-cyclen. Therefore, the covalent immobilization directly leads to the alteration of the coordination geometry of Cu(II) in this case. The logical assumption is that this new species with a somewhat distorted coordination geometry is the catalytically active component in the functionalized aerogel, because the hydrated [Cu(II)-cyclen]$^{2+}$ complex does not exhibit any SOD activity [41]. Apparently, the noted structural feature is strong enough under the applied conditions to compensate for the slightly negative Zeta potential of this functionalized aerogel in its reaction with superoxide.

Consequently, the most important factors responsible for the altered reactivities of the immobilized complexes compared to the aqueous ones are as follows. *i*) The formation of new chemical environments, i.e., new catalytically active complex species in the hydrated aerogels (confirmed by EPR) due to the covalent immobilization. *ii*) The effective separation of the active Cu(II) centers (confirmed by SANS and EPR). *iii*) The confinement effect operative in the nanoporous network. Similar conclusions were drawn when investigating the effect of nanoscale immobilization of open chain Cu(II) and bridged Cu(II)-Zn(II) complexes in layered double hydroxides and order mesoporous silicas [14,15].

Table 6
The IC_{50} values of aqueous and immobilized SOD mimetic systems. (The values in the present work are reported at pH = 7.60 and 25 °C).

	Description	IC_{50} (μM)	Ref.
[Cu(II)-cyclam]$^{2+}$	aqueous	26.1 ± 0.8	this work
[Cu(II)-cyclen]$^{2+}$	aqueous	N.A.	this work
CuClam-AG(immobilized Cu (II) -cyclam)	silica aerogel microparticle	1.7 ± 0.1	this work
CuClen-AG(immobilized Cu (II) -cyclen)	silica aerogel microparticle	2.1 ± 0.2	this work
Cu(II)-Zn(II)-imidazolato complex	aqueous	58	[17]
Cu(II)-Zn(II)-imidazolato complex in silica	mesoporous silica nanoparticle	1.9	[17]
Cu(II)-bipyridyl + Fe(III)-citrate in LDH	layered double hydroxide nanoclay	ca. 0.1	[13]
Cu(II)-PydiTyr complex	aqueous	0.028	[9]
CuZnSOD enzyme	aqueous	0.010	[9]

3.11. Perspectives for biomedical applications

A possible perspective for the use of the functionalized aerogel microparticles is their utilization as passive targeting antioxidant agents administered locally or subcutaneously. It has been shown before in several *in vitro* and *in vivo* studies that silica aerogel microparticles having slightly negative Zeta potentials under biologically relevant conditions are biocompatible and can normally be secreted by animals [26,42–44]. Therefore, antioxidant aerogel microparticles can be useful for the local treatment of inflammation or other oxidative stress related conditions. Furthermore, it was shown in a recent animal study that silica aerogel microparticles injected as a suspension into the abdominal cavity of mice enter the lymphatic circulation of the animals and accumulate in lymph nodes [45]. Therefore, the present antioxidant aerogel microparticles may be developed to be passive targeting agents for the systemic treatment of conditions associated with oxidative stress.

The present Cu(II)-macrocycles with 4 nitrogen donor atoms ensure the high stability and the kinetic inertness of the coordination of Cu(II), which is essential in biological systems where competitive ligands are abundant in the form amino acids, peptides, proteins and other biomolecules. Therefore, these immobilized complexes are excellent candidates for further *in vitro* and *in vivo* studies.

4. Conclusions

The copper(II) complexes of cyclen and cyclam were successfully immobilized using different covalent linkers in mesoporous silica aerogels. The chemical structures of the functionalized aerogels were elucidated based on the combined mass spectrometry (MS) and nuclear magnetic resonance spectroscopy (NMR) characterization of the synthetic precursors, and the electron paramagnetic resonance (EPR) spectroscopy characterization of the as-prepared aerogels. The presence of the covalent linkers alters the chemical environments of the complexes, which leads to a new coordination mode of Cu(II) in the pristine Cu(II)-cyclen functionalized aerogel compared to the parent complex. Contrast variation small angle neutron scattering (SANS) and EPR measurements unambiguously prove that the Cu(II)-complexes are not aggregated, but molecularly dispersed in the silica networks. The functionalized aerogel microparticles show excellent catalytic activities in the dismutation reaction of the superoxide anion mimicking the superoxide dismutase enzymes (SODs). Interestingly, the covalent immobilization drastically increases the SOD activities of both Cu(II) complexes compared to the aqueous parent complexes. This is the most remarkable

in the case of the Cu(II)-cyclen functionalized aerogel, because the aqueous complex does not show any activity. The most important factors responsible for the altered reactivities are as follows. *i*) The formation of new chemical environments and Cu(II) coordination modes due to the covalent immobilization. *ii*) The effective separation of the active Cu(II) centers in the aerogels. *iii*) The confinement effect operative in the nanoporous network. A general consideration in coordination chemistry is, that the immobilization of complexes in solid porous networks is advantageous for the stabilization of catalytically important intermediates and the inhibition of their intermolecular side reactions. A perspective for the future development of the functionalized aerogel microparticles is their utilization as passive targeting antioxidant pharmaceutical agents administered locally or subcutaneously.

Declaration of Competing Interest

The authors declare that they have no known competing financial interests or personal relationships that could have appeared to influence the work reported in this paper.

Data availability

Data will be made available on request.

Acknowledgements

This research has been financially supported by the National Research, Development and Innovation Office, Hungarian Science Foundation (OTKA: FK_17-124571 and K_21-139140). J. Kalmár is grateful for the János Bolyai Research Scholarship of the Hungarian Academy of Sciences and for the New National Excellence Program (ÚNKP-21-5 Bolyai+) of the Ministry of Innovation and Technology of Hungary for financial support.

Appendix A. Supplementary material

Supplementary material related to this article can be found in the online version of the article. Additional experimental details, including **Figures S1 to S16** referred to in the text. Characterization of the precursors, hydrolytic stability of the aerogels, SOD measurements.

Supplementary data to this article can be found online at https://doi.org/10.1016/j.apsusc.2022.155622.

References

[1] C. Nathan, A. Cunningham-Bussel, Beyond oxidative stress: an immunologist's guide to reactive oxygen species, Nat. Rev. Immunol. 13 (2013) 349–361, https://doi.org/10.1038/nri3423.
[2] Y. Sheng, I.A. Abreu, D.E. Cabelli, M.J. Maroney, A.-F. Miller, M. Teixeira, J. S. Valentine, Superoxide dismutases and superoxide reductases, Chem. Rev. 114 (2014) 3854–3918, https://doi.org/10.1021/cr4005296.
[3] A.-F. Miller, Superoxide dismutases: active sites that save, but a protein that kills, Curr. Opin. Chem. Biol. 8 (2004) 162–168, https://doi.org/10.1016/j.cbpa.2004.02.011.
[4] A. Umeno, V. Biju, Y. Yoshida, In vivo ROS production and use of oxidative stress-derived biomarkers to detect the onset of diseases such as Alzheimer's disease, Parkinson's disease, and diabetes, Free Radic. Res. 51 (2017) 413–427, https://doi.org/10.1080/10715762.2017.1315114.
[5] P. Newsholme, V.F. Cruzat, K.N. Keane, R. Carlessi, P.I.H. de Bittencourt Jr., Molecular mechanisms of ROS production and oxidative stress in diabetes, Biochem. J. 473 (2016) 4527–4550, https://doi.org/10.1042/bcj20160503c.
[6] A. El-Kenawi, B. Ruffell, Inflammation, ROS, and Mutagenesis, Cancer Cell 32 (2017) 727–729, https://doi.org/10.1016/j.ccell.2017.11.015.
[7] M.R. Filipović, A.C.W. Koh, S. Arbault, V. Niketić, A. Debus, U. Schleicher, C. Bogdan, M. Guille, F. Lemaître, C. Amatore, I. Ivanović-Burmazović, Striking Inflammation from Both Sides: Manganese(II) Pentaazamacrocyclic SOD Mimics Act Also as Nitric Oxide Dismutases: A Single-Cell Study, Angew. Chem., Int. Ed. Engl. 49 (2010) 4228–4232, https://doi.org/10.1002/anie.200905936.
[8] D. Lieb, F.C. Friedel, M. Yawer, A. Zahl, M.M. Khusniyarov, F.W. Heinemann, I. Ivanović-Burmazović, Dinuclear Seven-Coordinate Mn(II) Complexes: Effect of Manganese(II)-Hydroxo Species on Water Exchange and Superoxide Dismutase Activity, Inorg. Chem. 52 (2013) 222–236, https://doi.org/10.1021/ic301714d.
[9] R. Diószegi, D. Bonczidai-Kelemen, A.C. Bényei, N.V. May, I. Fábián, N. Lihi, Copper(II) Complexes of Pyridine-2,6-dicarboxamide Ligands with High SOD Activity, Inorg. Chem. 61 (2022) 2319–2332, https://doi.org/10.1021/acs.inorgchem.1c03728.
[10] G. Wu, E.A. McHugh, V. Berka, W.Y. Chen, Z. Wang, J.L. Beckham, P.J. Derry, T. Roy, T.A. Kent, J.M. Tour, A.L. Tsai, Oxidized Activated Charcoal Nanoparticles as Catalytic Superoxide Dismutase Mimetics: Evidence for Direct Participation of an Intrinsic Radical, ACS Appl. Nano Mater. 3 (2020) 6962–6971, https://doi.org/10.1021/acsanm.0c01285.
[11] M. Pavlovic, P. Rouster, I. Szilagyi, Synthesis and formulation of functional bionanomaterials with superoxide dismutase activity, Nanoscale 9 (2017) 369–379, https://doi.org/10.1039/C6NR07672F.
[12] P. Rouster, M. Pavlovic, I. Szilagyi, Immobilization of Superoxide Dismutase on Polyelectrolyte-Functionalized Titania Nanosheets, ChemBioChem 19 (2018) 404–410, https://doi.org/10.1002/cbic.201700502.
[13] Z. Somosi, N.V. May, D. Sebők, I. Pálinkó, I. Szilágyi, Catalytic antioxidant nanocomposites based on sequential adsorption of redox active metal complexes and polyelectrolytes on nanoclay particles, Dalton Trans. 50 (2021) 2426–2435, https://doi.org/10.1039/D0DT04186F.
[14] M. Pavlovic, B. Náfrádi, P. Rouster, S. Muráth, I. Szilagyi, Highly stable enzyme-mimicking nanocomposite of antioxidant activity, J. Colloid Interface Sci. 543 (2019) 174–182, https://doi.org/10.1016/j.jcis.2019.02.050.
[15] M. Patriarca, V. Daier, G. Camí, N. Pellegri, E. Rivière, C. Hureau, S. Signorella, Biomimetic Cu, Zn and Cu2 complexes inserted in mesoporous silica as catalysts for superoxide dismutation, Microporous Mesoporous Mater. 279 (2019) 133–141, https://doi.org/10.1016/j.micromeso.2018.12.027.
[16] C.-H. Lee, H.-C. Lin, S.-H. Cheng, T.-S. Lin, C.-Y. Mou, Hydroxo-Bridged Dinuclear Cupric Complexes Encapsulated in Various Mesoporous Silicas to Mimic the Catalytic Activity of Catechol Oxidases: Reactivity and Selectivity Study, J. Phys. Chem. C 113 (2009) 16058–16069, https://doi.org/10.1021/jp900156s.
[17] Y.-C. Fang, H.-C. Lin, I.J. Hsu, T.-S. Lin, C.-Y. Mou, Bioinspired Design of a Cu–Zn–Imidazolate Mesoporous Silica Catalyst System for Superoxide Dismutation, J. Phys. Chem. C 115 (2011) 20639–20652, https://doi.org/10.1021/jp207357x.
[18] T. Chen, X. Wang, Y. He, C. Zhang, Z. Wu, K. Liao, J. Wang, Z. Guo, Effects of cyclen and cyclam on zinc(II)- and copper(II)-induced amyloid beta-peptide aggregation and neurotoxicity, Inorg. Chem. 48 (2009) 5801–5809, https://doi.org/10.1021/ic900025x.
[19] J.D. Silversides, C.C. Allan, S.J. Archibald, Copper(II) cyclam-based complexes for radiopharmaceutical applications: synthesis and structural analysis, Dalton Trans. (2007) 971–978, https://doi.org/10.1039/b615329a.
[20] R.W. Hay, M.P. Pujari, The Dissociation of [Cu(Cyclen)]2+ in Acid-Solution - a Kinetic-Study, Inorg. Chim. Acta 100 (1985) L1–L3, https://doi.org/10.1016/S0020-1693(00)85272-X.
[21] K.S. Woodin, K.J. Heroux, C.A. Boswell, E.H. Wong, G.R. Weisman, W.J. Niu, S. A. Tomellini, C.J. Anderson, L.N. Zakharov, A.L. Rheingold, Kinetic inertness and electrochemical behavior of copper(II) tetraazamacrocyclic complexes: Possible implications for in vivo stability, Eur. J. Inorg. Chem. 2005 (2005) 4829–4833, https://doi.org/10.1002/ejic.200500579.
[22] H.F. Bereczki, L. Daróczi, I. Fabian, I. Lazar, Sol-gel synthesis, characterization and catalytic activity of silica aerogels functionalized with copper (II) complexes of cyclen and cyclam, Microporous Mesoporous Mater. 234 (2016) 392–400, https://doi.org/10.1016/j.micromeso.2016.07.026.
[23] I. Lazar, H.F. Bereczki, S. Manó, L. Daroczi, G. Deák, I. Fabian, Z. Csernátony, Synthesis and study of new functionalized silica aerogel poly (methyl methacrylate) composites for biomedical use, Polym. Compos. 36 (2015) 348–358, https://doi.org/10.1002/pc.22949.
[24] I. Lázár, I. Fábián, A continuous extraction and pumpless supercritical CO2 drying system for laboratory-scale aerogel production, Gels 2 (2016) 26, https://doi.org/10.3390/gels2040026.
[25] A. Forgács, Z. Balogh, M. Andrási, A. Len, Z. Dudás, N.V. May, P. Herman, L. Juhász, I. Fábián, N. Lihi, J. Kalmár, Mechanistic explanation for differences between catalytic activities of dissolved and aerogel immobilized Cu(II) cyclen, Appl. Surf. Sci. 579 (2022), 152210, https://doi.org/10.1016/j.apsusc.2021.152210.
[26] I. Lázár, A. Forgács, A. Horváth, G. Király, G. Nagy, A. Len, Z. Dudás, V. Papp, Z. Balogh, K. Moldován, L. Juhász, C. Cserháti, Z. Szántó, I. Fábián, J. Kalmár, Mechanism of hydration of biocompatible silica-casein aerogels probed by NMR and SANS reveal backbone rigidity, Appl. Surf. Sci. 531 (2020) 147232.
[27] G. Beaucage, Small-angle scattering from polymeric mass fractals of arbitrary mass-fractal dimension, J. Appl. Crystallogr. 29 (1996) 134–146, https://doi.org/10.1107/S0021889895011605.
[28] B. Hammouda, Analysis of the Beaucage model, J. Appl. Crystallogr. 43 (2010) 1474–1478, https://doi.org/10.1107/S0021889810033856.
[29] A. Rockenbauer, L. Korecz, Automatic computer simulations of ESR spectra, Appl. Magn. Reson. 10 (1996) 29–43, https://doi.org/10.1007/BF03163097.
[30] C. Beauchamp, I. Fridovich, Superoxide dismutase: Improved assays and an assay applicable to acrylamide gels, Anal. Biochem. 44 (1971) 276–287, https://doi.org/10.1016/0003-2697(71)90370-8.
[31] J.Y. Zhou, P. Prognon, Raw material enzymatic activity determination: A specific case for validation and comparison of analytical methods—The example of superoxide dismutase (SOD), J. Pharm. Biomed. 40 (2006) 1143–1148, https://doi.org/10.1016/j.jpba.2005.09.022.
[32] N. Lihi, D. Kelemen, N.V. May, I. Fábián, The Role of the Cysteine Fragments of the Nickel Binding Loop in the Activity of the Ni(II)-Containing SOD Enzyme, Inorg. Chem. 59 (2020) 4772–4780, https://doi.org/10.1021/acs.inorgchem.0c00057.

[33] M. Kéri, A. Forgács, V. Papp, I. Bányai, P. Veres, A. Len, Z. Dudás, I. Fábián, J. Kalmár, Gelatin content governs hydration induced structural changes in silica-gelatin hybrid aerogels–Implications in drug delivery, Acta Biomater. 105 (2020) 131–145, https://doi.org/10.1016/j.actbio.2020.01.016.
[34] N.H. Borzęcka, B. Nowak, R. Pakuła, R. Przewodzki, J.M. Gac, Cellular Automata Modeling of Silica Aerogel Condensation Kinetics, Gels 7 (2021) 50, https://doi.org/10.3390/gels7020050.
[35] M. Thommes, K. Kaneko, A.V. Neimark, J.P. Olivier, F. Rodriguez-Reinoso, J. Rouquerol, K.S. Sing, Physisorption of gases, with special reference to the evaluation of surface area and pore size distribution (IUPAC Technical Report), Pure Appl. Chem. 87 (2015) 1051–1069, https://doi.org/10.1515/pac-2014-1117.
[36] A. Otsuki, L. De Campo, C.J. Garvey, C. Rehm, H2O/D2O contrast variation for ultra-small-angle neutron scattering to minimize multiple scattering effects of colloidal particle suspensions, Colloids Interfaces 2 (2018) 37, https://doi.org/10.3390/colloids2030037.
[37] P. Paraskevopoulou, G. Raptopoulos, A. Len, Z. Dudas, I. Fabian, J. Kalmar, Fundamental Skeletal Nanostructure of Nanoporous Polymer-Cross-Linked Alginate Aerogels and Its Relevance To Environmental Remediation, ACS Appl. Nano Mater. 4 (2021) 10575–10583, https://doi.org/10.1021/acsanm.1c02072.
[38] A. Emmerling, J. Fricke, Small angle scattering and the structure of aerogels, J. Non-Cryst. Solids 145 (1992) 113–120, https://doi.org/10.1016/S0022-3093(05)80439-9.
[39] J. Kalmár, M. Kéri, Z. Erdei, I. Bányai, I. Lázár, G. Lente, I. Fábián, The pore network and the adsorption characteristics of mesoporous silica aerogel: adsorption kinetics on a timescale of seconds, RSC Adv. 5 (2015) 107237–107246, https://doi.org/10.1039/C5RA21353C.
[40] K. Miyoshi, H. Tanaka, E. Kimura, S. Tsuboyama, S. Murata, H. Shimizu, K. Ishizu, Electrochemical and spectroscopic studies on copper(II) complexes of macrocyclic ligands as models for square-pyramidal metal active sites of copper(II) complexes of bleomycin and glutathione, Inorganica Chim. Acta 78 (1983) 23–30, https://doi.org/10.1016/S0020-1693(00)86483-X.
[41] Á. Martínez-Camarena, A. Liberato, E. Delgado-Pinar, A.G. Algarra, J. Pitarch-Jarque, J.M. Llinares, M.Á. Mañez, A. Domenech-Carbó, M.G. Basallote, E. García-España, Coordination Chemistry of Cu2+ Complexes of Small N-Alkylated Tetra-azacyclophanes with SOD Activity, Inorg. Chem. 57 (2018) 10961–10973, https://doi.org/10.1021/acs.inorgchem.8b01492.
[42] J.P. Vareda, C.A. Garcia-Gonzalez, A.J.M. Valente, R. Simon-Vazquez, M. Stipetic, L. Duraes, Insights on toxicity, safe handling and disposal of silica aerogels and amorphous nanoparticles, Environ. Sci, Nano 8 (2021) 1177–1195, https://doi.org/10.1039/d1en00026h.
[43] M.A.A. Al-Najjar, T. Athamneh, R. AbuTayeh, I. Basheti, C. Leopold, P. Gurikov, I. Smirnova, A.K. Yadav, Evaluation of the orally administered calcium alginate aerogel on the changes of gut microbiota and hepatic and renal function of Wistar rats, PLoS One 16 (4) (2021) e0247633.
[44] P. Veres, G. Kiraly, G. Nagy, I. Lazar, I. Fabian, J. Kalmar, Biocompatible silica-gelatin hybrid aerogels covalently labeled with fluorescein, J. Non-Cryst. Solids 473 (2017) 17–25, https://doi.org/10.1016/j.jnoncrysol.2017.07.016.
[45] G. Kiraly, J.C. Egu, Z. Hargitai, I. Kovacs, I. Fabian, J. Kalmar, G. Szeman-Nagy, Mesoporous Aerogel Microparticles Injected into the Abdominal Cavity of Mice Accumulate in Parathymic Lymph Nodes, Int. J. Mol. Sci. 22 (2021) 9756, https://doi.org/10.3390/ijms22189756.